Mass-Independent Oxygen Isotope (^{16}O, ^{17}O, ^{18}O) Fractionation Found in H_x, O_x Reactions

Joel Savarino* and Mark H. Thiemens

University of California, San Diego, Department of Chemistry Mail Code 0356, 9500 Gilman Drive, La Jolla, California 92093-0356

Received: April 14, 1999; In Final Form: July 13, 1999

The oxygen isotopic composition (^{16}O, ^{17}O, ^{18}O) of the products produced in H_x, O_x reactions has been investigated using a fast flow reactor. The products were trapped at liquid nitrogen temperature. Measurement of all stable oxygen isotopes on reaction products enhanced distinction between mass-dependent and mass-independent fractionation processes. It was observed that all product species were mass-independently fractionated (MIF). Kinetic analysis suggests that MIF may derive from the H + O_2 + M reaction. Kinetic analysis and discussion of the potential role of symmetry reactions are presented. The similarity of isotopic behavior between this reaction and ozone formation suggests a common origin. Currently, no theory explains the mass-independent fractionation observed in any gas-phase chemical reaction. Due to its atmospheric importance, possible isotopic implications for the Earth's atmosphere are discussed.

Introduction

The discovery in 1983 of an unusual enrichment in the isotopes ^{17}O, ^{18}O in ozone was observed in an electrical discharge in molecular oxygen[2] and was later observed in stratospheric ozone.[3,4] These two works initiated experimental and theoretical studies on this new isotope fractionation process.[5−11] The mechanism responsible for this effect, termed mass-independent fractionation (MIF), remains elusive. Despite this, numerous applications of MIF exist in atmospheric chemical studies (see recent review by Thiemens[12] and Weston[13]).

Conventional mass-dependent isotopic fractionations arise as a result of small differences in mass between isotopomers which subsequently produce small differences in translational velocity and bond strength. The former is responsible for most of the physicochemical differences between isotopic species (diffusion rates, condensation, vapor pressure), and the latter for kinetic and equilibrium isotope effects. Variations in isotope ratios are defined using the conventional δ notation,[14] which for oxygen isotopes is

$$\delta^{17}O(‰) = \left[\frac{(^{17}R_{sample})}{(^{17}R_{std})} - 1\right] 1000$$

$$\delta^{18}O(‰) = \left[\frac{(^{18}R_{sample})}{(^{18}R_{std})} - 1\right] 1000$$

where δ represents the variation in parts per thousand of isotopic ratio $^{17}R = {}^{17}O/{}^{16}O$ and $^{18}R = {}^{18}O/{}^{16}O$ of a sample relative to a standard material. Mass-dependent processes obey the relation

$$\delta^{17}O \approx 0.5\,\delta^{18}O$$

This is because the mass difference for $\delta^{18}O$ is 2, and for $\delta^{17}O$ is 1, thus any alteration of the isotope ratio for $\delta^{18}O$ concomitantly produces a change ~1/2 that of $\delta^{17}O$. Experimental measurements of terrestrial and lunar solid materials and water samples have confirmed this relation.[15] However, there are some gas-phase chemical reactions which produce mass-independent isotopic compositions[2,5,7,11,16,17] such that $\delta^{17}O \neq 0.5\,\delta^{18}O$. A recent observation of a mass-independent composition in rainwater hydrogen peroxide,[18] a major atmospheric oxidant, has initiated the following experiments. There exists a high probability that this unique isotopic signature may be used to trace, for instance, the many sulfur oxidation pathways in the atmosphere of Earth and possibly Mars.

The major natural and anthropogenic source of atmospheric H_2O_2 is generally thought to be the gas-phase recombination of HO_2 radicals[19,20]

$$HO_2 + HO_2 \rightarrow H_2O_2 + O_2 \qquad (1)$$

Since most HO_2 radicals derive from the photochemical production of OH, any unusual isotopic signature of one of the species H_2O_2, HO_2, or OH may offer new insight into their budgets, cycles, and interactions.

A great deal of effort has been devoted to the H_2-O_2 system, primarily to probe reactions at explosion limits (for a exhaustive review prior to 1967 see Venugopalan and Jones[1]). Reaction kinetics were determined by measurement of stable products. More recently, the emergence of the fields of atmospheric chemistry and planetology have stimulated an intensive effort to quantify the reactions involved in the H_2-O_2 system.[21−26] Regardless of the initiating step in the oxidation of hydrogen (e.g., thermal, photochemical, electrical discharge, radiochemical reactions), the reaction of O_2 with H_2 leads to the formation of three stable products at room temperature: O_3, H_2O_2, and H_2O.[27,28] The relative proportions of each species depend on the ratio of H_2/O_2, the initiation reaction step, and more generally, the design and experimental configuration.[1] The reaction between hydrogen and oxygen involves the formation and disappearance of the species H, O, OH, and HO_2, all significant radicals in atmospheric chemistry[29] and combustion reactions.[30,31] Unstable hydrogen superoxides (hydrogen trioxide, H_2O_3, and tetroxide, H_2O_4) have also been identified at temperatures below 160 K.[32−35] It is well established that

* E-mail: joel@chem.ucsd.edu, mht@chem.ucsd.edu.

10.1021/jp991221y CCC: $18.00
Published on Web 11/03/1999

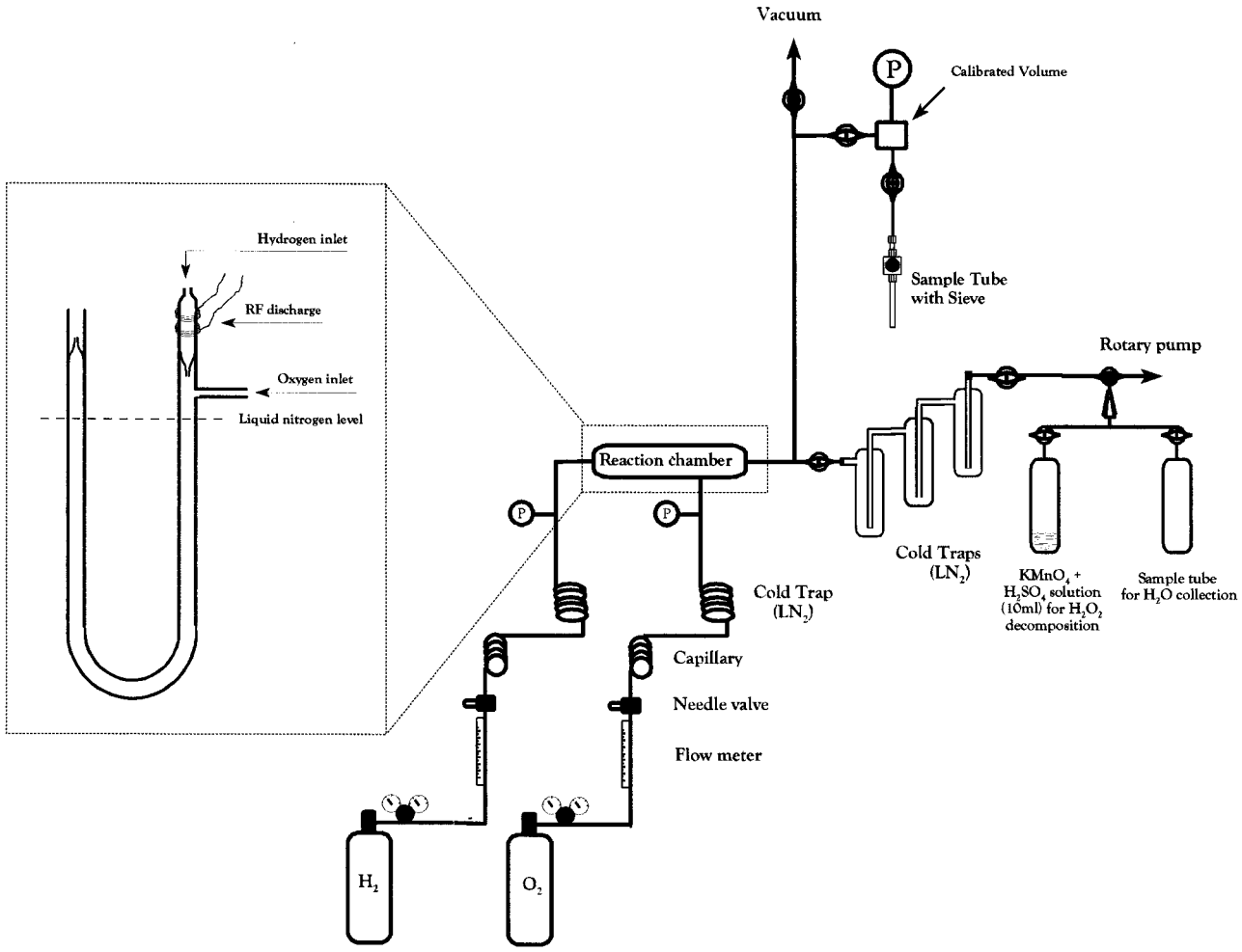

Figure 1. Experimental line design to study the oxygen isotopic ratios of the products of the $H + O_2 + M$ reaction. The nozzle ensures a relative pressure independency between compartments.

decomposition of these superoxides leads to the formation of O_2, H_2O, and H_2O_2.[1,36]

The present paper examines the H_2-O_2 reaction system at the isotopic level. The potential application and interpretation of the observed atmospheric hydrogen peroxide isotopic measurements is limited by the lack of relevant isotopic measurements in the $H_2-O_2-H_2O_2$ system. The present measurements alleviate this limitation and provide data which may be applied to the atmospheric observations.

Experimental Section

A schematic representation of the experimental apparatus is shown in Figure 1. The system initiates the oxidation of the hydrogen molecules according to the reaction

$$H + O_2 + M \rightarrow HO_2 + M \qquad (2)$$

with the hydrogen atoms produced by electron impact in an hydrogen plasma. The stable products are collected for oxygen isotopic analysis. Unless otherwise noted, all traps and molecular sieves were cooled at liquid nitrogen temperature. Cryotransfer was accomplished at this temperature.

For the experiments, high purity hydrogen (Matheson, 99.99%) and oxygen (Matheson, 99.993%) were used. Two blank experiments were conducted to ensure that stable products collected in the cold trap were the consequence of reaction 2. For the first blank no discharge was applied and O_2 and H_2 were flowing at typical flow rates (mmol min^{-1} range) for half an hour. For the second blank, only H_2 was flowing through the system and the discharge was ignited. In both cases, the total condensable product at liquid nitrogen temperature was less than 0.1 μmol.

A double stage regulator on both tanks maintained inlet pressure at 3.5 atm. Gas flow rates were measured using two rotameters (Omega Inc.) and converted to STP by correction for gas density and inlet pressure. Typical flow rates range from 0.9 μmol min^{-1} to 2.7 mmol min^{-1} for O_2, corresponding to a partial pressure between 0.1 and 6.7 Torr in the reaction chamber. For H_2, the flow rate was kept constant at 21 mmol min^{-1}. The discharge pressure zone, monitored by a capacitance pressure gauge (MKS Baratron), was 20.0 ± 1.0 Torr and was insensitive to O_2 flow due to the presence of a venturi. Total pressure in the reaction chamber was 7 Torr oxygen free, and increased to a maximum pressure of 13.5 Torr with O_2 present.

Precise valve control and a capillary were utilized to regulate flow and restrict gas back diffusion during the mixing step. A cold trap was placed just after the capillary to remove any trace of water in the gas stream before entering the reaction chamber.

An expanded view of the reaction chamber is also shown in Figure 1. The reaction chamber is quartz and consists of a U trap (i.d. 10 mm) with two inlets, one for H_2 and enclosed by an RF discharge antenna. Hydrogen atoms were carried by the H_2 carrier gas out of the zone of high-voltage discharge through the nozzle, and into the reaction chamber. The power of the RF generator (ENI Power System Inc.) was constant at 20 W for all experiments.

TABLE 1: Experimental Flow Conditions and Measured Production Rates of H_2O_2 and O_2* (see text for O_2* definition) along with Their Ratio and O_2 Yield

run	tot press (Torr)	O_2 flow (μmol min^{-1})$_{STP}$	time (min)	prod rate of H_2O_2 (μmol min^{-1})	prod rate of O_2* (μmol min^{-1})	H_2O_2/O_2*	yield of O_2 recovered from H_2O_2 and O_2*
1	7.23	0.9	160	0.5	0.1	5.0	0.67
2	7.26	1.9	45	0.9	0.2	4.5	0.65
3	7.27	2.0	75	0.9	0.2	4.5	0.61
4	7.3	3.6	30	2.0			
5	7.36	6.2	10	2.9			
6	7.42	9.5	9	5.6			
7	7.42	10.0	10	5.5	1.6	3.4	0.79
8	7.50	13.6	15	3.8	2.0	1.9	0.43
9	7.40	13.5	15	3.8			
10	7.60	24.3	10	2.7	2.3	1.2	0.23
11	7.80	47.8	15	2.4	2.8	0.9	0.12
12	8.15	103.6	11	1.9	1.6	1.2	0.04
13	8.6	207.8	20	1.7	1.6	1.1	0.02
14	8.6	211.3	20	1.5	1.4	1.1	0.01
15	8.80	265.5	25	0.8	0.8	1.0	0.01
16	9.87	669.3	30	0.9	0.7	1.3	0.00
17	11.53	1595	40	0.3	0.3	1.0	0.00
18	13.51	3063	35	0.6			

[a] For some experiments, O_2* was not measured since the initial experiments were directed toward H_2O_2 analysis.

The oxidation products of the hydrogen initiated reaction were trapped directly in the reaction chamber and in three sequential traps placed approximately 30 cm downstream. Collection protocols were the same for all samples. At vacuum conditions ($<10^{-3}$ Torr), the collection traps are cooled and the gases introduced at the desired flow rate. The system is then switched to a double stage rough pump (10^{-3} Torr). After attaining equilibrium, RF dissociation of H_2 is initiated. The reaction proceeds until sufficient product is formed for high precision isotopic analysis (typically between 5 min to 1 h for $\sim$20 μmol of H_2O_2, depending on the rate of production). The injectors are closed at reaction termination and the system evacuated. In all experiments, condensable products were visible and formed a layer at the liquid nitrogen level. No experiment produced sufficient O_3 to be visible. All traps are thawed and the products transferred to two sample tubes at liquid nitrogen temperature. One tube contained an acidic solution of excess potassium permanganate, free of dissolved gas, to decompose H_2O_2. The second one was eventually used for water isotope measurements. After the water and hydrogen peroxide have been trapped, any residual molecular oxygen from thermal decomposition of unstable superoxide is transferred to a molecular sieve (13X) at liquid nitrogen temperature. O_2* denotes molecular oxygen released from hydrogen superoxide decomposition. This notation is to distinguish between this molecular oxygen and the flow O_2.

To make $\delta^{17}O$ measurements, all molecules must be converted to O_2. The hydrogen peroxide is decomposed by potassium permanganate and the released oxygen transferred to a sample tube after volumetric determination. It has been demonstrated that oxygen released during this reaction derives only from H_2O_2[37] and that no oxygen isotope exchange occurs between H_2O_2 and the other compounds.[37−39] Recently, this method has been successful in the isotopic analysis of rainwater H_2O_2.[18,40] Water is reacted with BrF_5 to quantitatively decompose water to HF and O_2. However, H_2O_2 and H_2O cannot be cryogenically separated, thus both are transferred to a Ni tube along with an excess of BrF_5. The Ni tube is closed and heated to 575 K for 2 h. The tube is then frozen to 77 K, the released molecular oxygen transferred to a molecular sieve at 77 K and measured for yield and isotope ratios. Only experiments where the production of H_2O exceed H_2O_2 by a few orders of magnitude were analyzed for isotopic ratios. In this case, the contribution of the hydrogen peroxide to the oxygen isotopic ratios can be neglected.

Accuracy of yield determination is estimated to be $\pm$10%. The uncertainty of the isotopic ratios ($\pm$ 2 ‰) was limited by experimental reproducibility rather than the mass spectrometric precision ($\pm$ 0.2 ‰). Isotope ratio measurements were performed on a dual inlet, triple collector isotope ratio mass spectrometer (Finnigan MAT 251).

Results

Kinetic Observations. Table 1 presents the experimental data for the production rate of H_2O_2 and O_2* (released during the warming stage), the ratios H_2O_2/O_2*, and the oxygen yield for both products. The total cell pressure does not influence production rates. Table 1 shows that for experiments 1 through 6, total pressure varied only by 2.6%, while the H_2O_2 production rate varies by a factor of 14. For the same experiments, the flow of O_2 in the system varies by a factor of 10, showing that it is this parameter which controls the rate of hydrogen peroxide formation. The quantitative yield of O_2 recovery is very high at low O_2 flow. Taking into account only H_2O_2 and O_2*, the yield may be as high as 80%. During these experiments (runs 1 to 6) all oxygen is consumed, and the formation of water accounts for the missing amount. At high flow O_2 recovery is only 2.5%, even if water is taken into account. From Table 1, it is also evident that H_2O_2 and O_2* production rates increase with O_2 flow to a maximum and then decrease. Figure 2 illustrates this behavior for H_2O_2. At low O_2 flow, the rate of formation is linear to the flow (Figure 2a) and 57% of the O_2 injected is found in H_2O_2. Above an O_2 flow rate of 10 μmol min^{-1}, the production rate of H_2O_2 decreases exponentially (Figure 2b). A similar feature has also been reported for water production.[41]

O_2* exhibits a different behavior than H_2O_2 at low flow, but similar at high flow (not plotted). The amount of O_2* released during the warming stage increases exponentially at low flow, and at enhanced flow exponentially decreases, as does H_2O_2. The threshold between low and high flow is, however, not the same for H_2O_2 and O_2, and values are 20 μmol min^{-1} and 43 μmol min^{-1}, respectively.

Figure 3 displays the varying H_2O_2/O_2* with oxygen flow. For flows lower than 20 μmol min^{-1}, the ratios are above 1, but converge to 1 for high flow conditions.

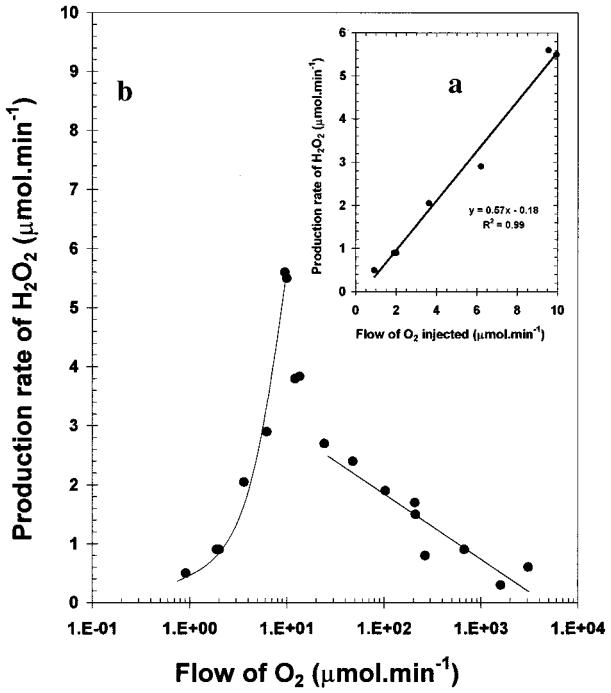

Figure 2. Production rate of H_2O_2 as a function of O_2 flow. Figure 2a is a linear *X*-axis plot showing the linear dependency of H_2O_2 production rate in the low flow regime of O_2. Figure 2b is plotted in a log *x*-axis to cover the total range.

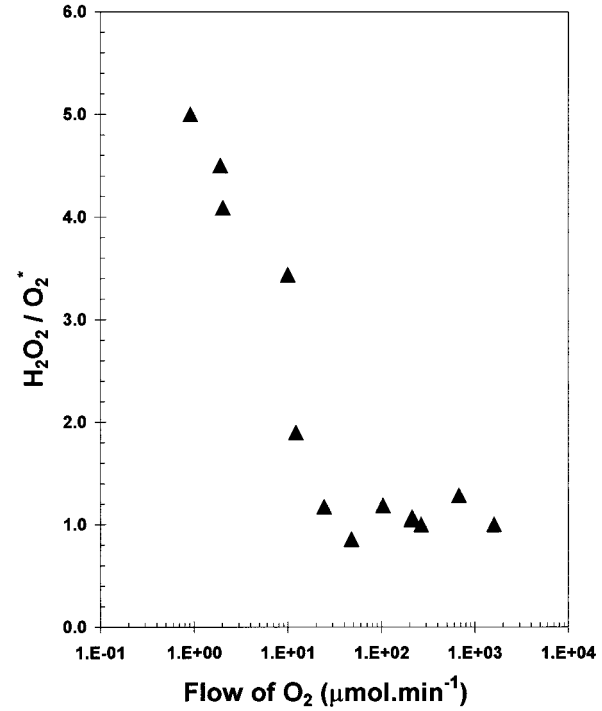

Figure 3. Plot of H_2O_2/O_2* versus O_2 flow. The data display the two flow regimes.

Isotopic Chemistry. Oxygen isotopic ratios of the products are given in Table 2 along with the ratios H_2O_2/O_2*. Here, $^{17}\Delta$ is a measure of the enrichment (or depletion) in ^{17}O relative to the conventional mass-dependent isotopic fractionation processes. It is defined as

$$^{17}\Delta = \delta^{17}O - 0.513 * \delta^{18}O$$

and $^{17}\Delta$ is thus the deviation from a mass dependent process.

TABLE 2: Isotopic Ratios for H_2O_2 and O_2* Obtained during the H + O_2 + M Reaction[a]

		H_2O_2			O_2*		
run	H_2O_2/O_2*	$\delta^{18}O_{tank}$	$\delta^{17}O_{tank}$	$^{17}\Delta$	$\delta^{18}O_{tank}$	$\delta^{17}O_{tank}$	$^{17}\Delta$
1	5.0	−19.2	−21.8	−12.0	−7.3	−15.3	−11.3
2	4.5	−21.1	−22.4	−11.6	−9.7	−15.7	−10.7
3	4.5	−10.3	−15.7	−10.4	−6.7	−13.3	−9.8
4		−9.6	−14.6	−9.7			
5		−19.6	−18.7	−8.6			
6		−23.2	−18.5	−6.6			
7	3.4	−3.5	−7.8	−6.0	−6.0	−8.1	−5.0
8	1.9	−6.8	−12.3	−8.8	−6.9	−11.8	−8.2
9		−1.8	−8.6	−7.6			
10	1.2	11.8	5.3	−0.7	6.1	2.8	−0.3
11	0.9	16.0	10.6	2.4	22.9	14.0	2.3
12	1.2	24.8	18.3	5.6	32.2	21.9	5.4
13	1.1	29.6	19.6	4.5	31.0	20.2	4.3
14	1.1	29.6	19.2	4.1	38.4	25.1	5.4
15	1.0	31.6	21.3	5.1	45.3	36.2	13.0
16	1.6	35.9	29.2	10.8	50.1	40.8	15.1
17	1.0	53.9	40.8	13.1	58.0	44.7	15.0
18		55.4	41.9	13.5			

[a] $\delta^x O_{tank}$ are expressed using the composition of the O_2 tank as the standard reference.

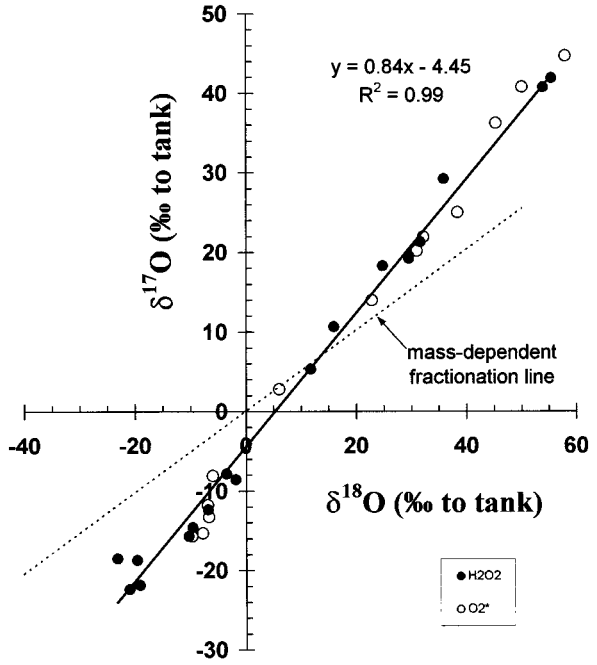

Figure 4. Three oxygen isotope plot of H_2O_2 and O_2*. The dotted line represent the mass-dependent fraction line, while the full line represents the best fit of H_2O_2 data. O_2* data lies along the same fractionation line.

For a mass-dependent fractionation, $^{17}\Delta = 0$. The coefficient 0.513 has been experimentally determined by measurement of different commercially available hydrogen peroxide solutions.[42] The isotope ratios are expressed relative to the flow gas oxygen.

It may be observed in Table 2 that hydrogen peroxide and product oxygen are both mass independently fractionated. The $\delta^{18}O$ and $\delta^{17}O$ composition of the product H_2O_2, relative to initial O_2, ranges between −20‰ and 55‰. The observed fractionation range is nearly the same as observed in ozone formation.[6,43] Figure 4 shows the isotopic composition of the products in a three isotope plot of $\delta^{17}O$ versus $\delta^{18}O$. The best-fit line of H_2O_2 data has a slope of 0.84 with a *y*-intercept at −4.45 and $r = 0.99$. The O_2* data fit the best-fit slope of H_2O_2 data. The results are evidence of a mass-independent fraction-

ation in a reaction other than ozone formation,[2] CO oxidation by O,[7] CO oxidation by OH,[11] and CO_2 photodissociation.[44]

H_2O_2 is heavy isotope depleted relative to initial O_2 ($\delta^{17}O$ and $\delta^{18}O < 0$) at low flow, while it is enriched at high flow ($\delta^{17}O$ and $\delta^{18}O > 0$). A similar behavior has been previously reported in the static[5] and dynamic formation of ozone.[43]

Discussion

Kinetic Chemistry. The interpretation of the isotopic data is enhanced by decades of experimental studies of the H_2-O_2 system. In particular, the $H + O_2$ reaction has received considerable attention. In the analysis of the isotopic data, the following observations must be accounted for:

(1) Hydrogen peroxide formation is not observed when the temperature of the cold trap exceeds 160 K.[45] An experiment was conducted for which the protocol was exactly the same as a sample except the temperature of the collection traps was 173 K, not 77 K. No H_2O_2 formation was observed.

The observation of no H_2O_2 in the collection traps at temperatures above 160 K is not due to trapping inefficiency or decomposition of H_2O_2 on the wall by H reaction or collision. McKinley and Garvin[46] have distilled hydrogen peroxide through their system at flow rates and pressures comparable to our discharge experiments and have recovered the peroxide completely in a trap at 193 K. Nor is the appearance of water in the traps due to decomposition of trapped peroxide by reaction with atomic hydrogen. Addition of ethylene at varying distances from the mixing zone indicated that most peroxide is formed on the cold wall of the trap.[47] Therefore, gas-phase disproportionation of HO_2 (reaction 1) as a significant source of hydrogen peroxide is ruled out.

(2) Hydrogen trioxide (H_2O_3) and tetroxide (H_2O_4) production are known to occur and should condense on the cold wall. Their decomposition initiates at temperature above 160 K producing H_2O_2 or H_2O and O_2*.[1]

(3) In certain circumstances, depending on the geometry and flow condition of the system, the ratio of $H_2O_2/O_2^* = 1$, which suggests that the source of H_2O_2 in these systems is from decomposition of H_2O_4.[1]

(4) Water is always a product, regardless of trap temperature,[41] and water formation inside the pre-trap zone has been established and also observed in previous experiments.[46,47]

These observations and the present isotopic measurements may be accommodated by the following proposed reaction scenario.

Chain initiation:

$$H_2 + e^- \rightarrow 2H + e^- \quad \text{(plasma breakdown)} \tag{3}$$

$$H + O_2 + M \rightarrow HO_2 + M \tag{2}$$

Alternative to reaction 2:

$$H + O_2 \rightarrow OH + O \tag{4}$$

However, reaction 4 is considered unimportant for several reasons. This reaction is well known to be one of the most important reactions in combustion chemistry;[48] however, it is activated only at high temperature. The high activation energy of reaction 4 ($E_a = 62.2$ kJ)[31] renders it improbable at room temperature. A kinetic analysis shows that the total pressure in the reaction chamber in the present experiments exceeds the pressure limit where reaction 4 dominates reaction 2. Utilizing the rate constants k_4 and k_5 given by Baulch et al.[31] and a total pressure of 8 Torr, reaction 2 is 6×10^6 times faster than reaction 4. Finally, ozone was not detected in the products frozen at liquid nitrogen temperature, suggesting that reactions producing O atoms are unimportant in this reducing environment.

Therefore, the reactions which occur in the reaction zone prior to trapping may be as follows (assuming that O atoms are unimportant):

$$H + HO_2 \rightarrow 2OH\ (90\%) \tag{5a}$$

$$H + HO_2 \rightarrow H_2 + O_2\ (10\%) \tag{5b}$$

$$OH + H + M \rightarrow H_2O + M \tag{6}$$

$$OH + H_2 \rightarrow H_2O + H \tag{7}$$

$$OH + HO_2 \rightarrow H_2O + O_2 \tag{8}$$

$$H + H + M \rightarrow H_2 + M \tag{9}$$

No reaction producing H_2O_2 has been included based upon previous work.[45−47] Reactions 5a and 5b are expected since H atoms occur in high concentration. If reaction 5b can be disregarded for our proposes (in a bath of O_2 and H_2, this reaction can be seen like a chain termination), reaction 5a is required to explain the formation of OH radical, which, in turn is necessary for water production. Reactions 6, 7, 8, and 9 complete the water scheme. Water formation is dominated by reactions 6−8, which vary in importance depending upon the amount of O_2 injected in the system.

The reactions which become important in the cryotrap include:

$$H + HO_2 + \text{wall} \rightarrow H_2O_2 + \text{wall} \tag{10}$$

$$OH + OH + \text{wall} \rightarrow H_2O_2 + \text{wall} \tag{11}$$

$$HO_2 + HO_2 + \text{wall} \rightarrow H_2O_4 + \text{wall} \tag{12}$$

$$H + OH + \text{wall} \rightarrow H_2O + \text{wall} \tag{13}$$

$$OH + HO_2 + \text{wall} \rightarrow H_2O_3 + \text{wall} \tag{14}$$

With the exception of reactions 11 and 12, all reactions are the heterogeneous equivalent of the gas-phase reactions in the pre-trap zone, with excess energy absorbed by the cold wall for complex stabilization. Formation of product must occur at this low temperature by a reaction of a negative activation energy. Reactions 11 and 12 have been proposed to explain the formation of hydrogen peroxide at temperatures initiating below 113 K,[1] with H_2O_4 clearly identified by Raman spectrometry.[32−35] Reaction 12 is of particular interest since it is this reaction that is in part responsible for the O_2 released and produces a ratio of $H_2O_2/O_2^* = 1$.

During the warming of the trap, the following reactions occur:

$$H_2O_4 \xrightarrow{\Delta} H_2O_2 + O_2 \tag{15}$$

$$H_2O_3 \xrightarrow{\Delta} H_2O + O_2 \tag{16}$$

Reaction 16 is probably unimportant in our system. Indeed, the ratios of H_2O_2/O_2^* are never lower than 0.9, demonstrating that there is no source of O_2* other than reaction 15.

Previous work from Badin et al.[41] and the present results (see Figure 2a) demonstrate that, in the low flow regime, accumulation of H_2O_2 in the cold trap is a linear function of injected O_2

and the corresponding ratio H_2O_2/O_2* exceeds 1 (Figure 3). Therefore, reaction 12 and its subsequent thermal decomposition (reaction 15) are not responsible for the formation of all H_2O_2 in the cold trap at these flows. Indeed, if reaction 12 was the only source of H_2O_2, the production of H_2O_2 should be proportional to the square of O_2 injected and the ratio H_2O_2/O_2* equal to 1, which is clearly not the case. Considering that oxygen recovery is around 80%, based only on H_2O_2 and O_2*, it is apparent that H atoms are in excess at the low pressure. This is consistent with observations of McKinley and Garvin[46] who have shown that complete oxygen recovery was obtained only when at least a 2.5-fold excess of atomic hydrogen (relative to O_2) was present in the reaction chamber. Under conditions where H atoms are abundant, it becomes apparent that reactions 10 and 11 are the other sources of H_2O_2 and that these sources dominated all other since H_2O_2/O_2* exceeds 1. The reaction mechanism is then restricted to the following reactions at low flow regime when $H > O_2$:

$$H + O_2 + M \rightarrow HO_2 + M \quad (2)$$

$$H + HO_2 \rightarrow 2OH \quad (5a)$$

$$H + HO_2 + \text{wall} \rightarrow H_2O_2 + \text{wall} \quad (10)$$

$$OH + OH + \text{wall} \rightarrow H_2O_2 + \text{wall} \quad (11)$$

Applying steady-state conditions for HO_2 and OH, one arrives at the simple expression

$$\frac{d[H_2O_2]}{dt} = \frac{(k_3k_1[W]2k_2k_1)}{(k_2k_3[W])}[O_2][M][H]$$

where k_i is the kinetic constant of ith reaction, [W] the third body wall, and [M] the third body gas. This indicates that, with an excess of atomic hydrogen and constant wall conditions as in the present experiments, the rate of peroxide formation is proportional to oxygen concentration. This is demonstrated at low oxygen concentration when the O_2 flow is lower than 10 μmol min^{-1} (Figure 2a). Nevertheless, it is not possible to distinguish which reaction, 10 or 11, dominates H_2O_2 formation during low flow conditions.

At higher O_2 flow ($>$20 μmol min^{-1}), the ratio H_2O_2/O_2* = 1, suggesting that reaction 12 followed by reaction 15 is the only mechanism for H_2O_2 production. As H atoms become low in number density, they are removed in the pre-trap chamber, suppressing reactions 10 and 11 in the cold trap. Simultaneous production of H_2O_2 strongly decreases with increasing O_2. There are two possibilities to account for this observation. Either peroxide formation decreases when water formation increases, or some H atoms are lost by reactions 5b and 9. In his original paper, Badin[41] observed a decrease in water formation and suggested that reaction 9 dominates. However, the present water experiments demonstrate that water formation increases with enhanced O_2. A possible explanation for the discrepancy between Badin and the present results may be the trapping efficiency. Badin[41] used only one cold trap to condense water and the present utilized three. In the present experiments, at high O_2 flow, the water product is always observed in the second trap. Therefore, the decreased H_2O_2 production probably arises from increased water production via formation of OH radicals.

Isotopic Chemistry. As observed in Figure 4, two main features arise from the experiments. First, the chain reaction sequence initiated by $H + O_2 + M$ ultimately produces a mass-independent fractionation in H_2O_2 and O_2*. Second, the best fit of the data does not pass through the initial isotopic composition, thus requiring participation of at least two fractionation processes of differing $\delta^{17}O/\delta^{18}O$. Individual reactions must be considered to identify the mass-independent source.

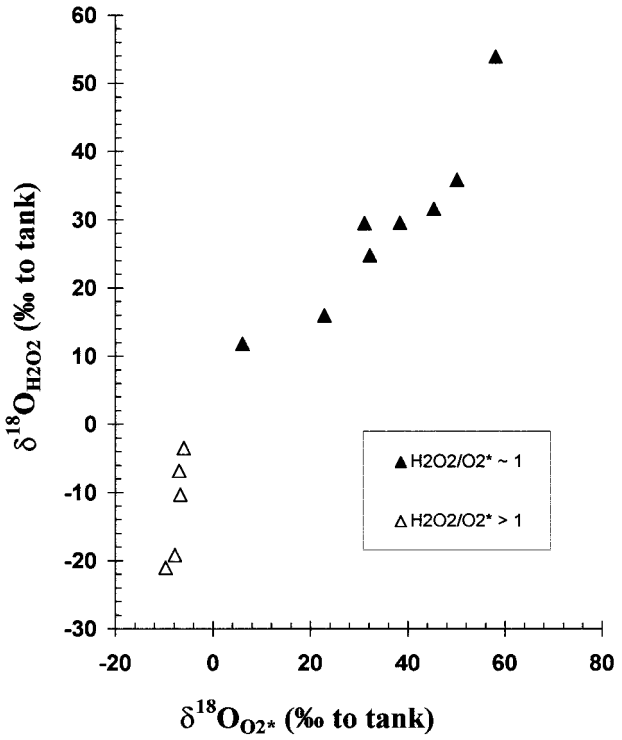

Figure 5. Correlation between $\delta^{18}O$ of H_2O_2 and $\delta^{18}O$ of O_2*. This plot reveals the two flow regimes: at the low regime, where $\delta^{18}O$ of H_2O_2 and $\delta^{18}O$ of O_2* are well correlated when $H_2O_2/O_2* \approx 1$, and at the high regime, where $\delta^{18}O$ of H_2O_2 and $\delta^{18}O$ of O_2* are not correlated when $H_2O_2/O_2* > 1$.

A possible candidate reaction is the thermal decomposition of H_2O_4 (reaction 15); however, this reaction may be rejected by mass balance considerations. Assuming a mass-dependent composition for H_2O_4 ($^{17}\Delta_{H2O4} = 0$), if its thermal decomposition was a mass-independent process, one of the products should be depleted in ^{17}O ($^{17}\Delta < 0$) while the other should be enriched in the opposite direction ($^{17}\Delta > 0$) to maintain material isotopic balance. From Table 2, this is clearly not the case.

The formation of H_2O_4 via reaction 12 is another candidate to account for the observations. Figure 5 is a plot of $\delta^{18}O$ of O_2* versus $\delta^{18}O$ of H_2O_2. For samples where $H_2O_2/O_2* = 1$, $\delta^{18}O$ for the two species are well correlated. This behavior is expected since H_2O_2 and O_2* are chemically linked by the succession of reactions 12 and 15, thus, the fractionation between H_2O_2 and O_2* is constant, implying a linear relationship between H_2O_2 and O_2*. On the other hand when $H_2O_2/O_2* > 1$, the $\delta^{18}O$ of H_2O_2 is independent of $\delta^{18}O$ of O_2*, the latter possessing a constant $\delta^{18}O$. This observation suggests that at low flow, the main source of H_2O_2 is not the H_2O_4 adduct, therefore decoupling the isotopic signature of H_2O_2 and O_2*. As detailed in the previous section, reactions 10 and 11 are the most probable sources of hydrogen peroxide. However, hydrogen peroxide lies on the same isotopic fractionation line whether reactions 10 and 11 or reaction 12 are the source of the peroxide, suggesting that H_2O_4 formation is not the source of the mass-independent fractionation. This is consistent with other experiments.[49] Utilizing an ^{18}O labeling technique to study H_2O_2 formation via the H_2O_4 adduct, their results demonstrated that isotopic exchange does not occur between $H^{16}O^{16}O$ and

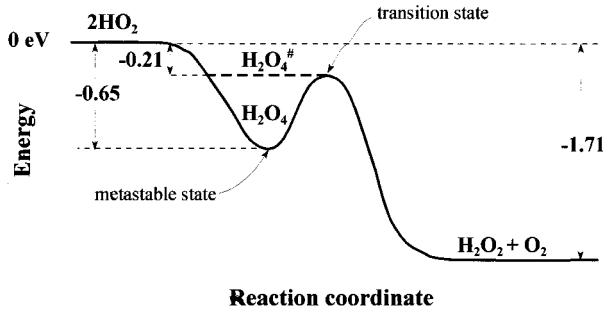

Figure 6. Schematic potential energy surface for self-reaction of HO_2 (adapted from ref 49). Energies are in eV.

$H^{18}O^{18}O$. Thus, even if the reaction proceeds via formation of a complex as shown in Figure 6, the mechanism behaves as a hydrogen abstraction by one of the two hydroperoxide radicals. Niki et al.[49] results imply that if HO_2 radicals were mass-dependently fractionated, the product H_2O_4 should also be mass-dependent fractionated since no oxygen isotope exchange occurs. Niki et al.[49] and the present results imply that the mass-independent fractionation observed in H_2O_2 and O_2* derives from the formation of HO_2. Observation of Niki et al.[49] and ab initio calculations[50] have suggested a possible symmetric dimer structure for the transition state $H_2O_4^{\#}$ (point group C_{2h}). Since the present results suggest that HO_2 possesses the MIF, the possible symmetric structure of $H_2O_4^{\#}$ does not appear to be involved in the MIF. This is consistent with a recent investigation of ozone formation (point group C_{2v}), which has questioned the role of molecular symmetry as the source of the mass-independent effect.[51] From the preceding analysis, it appears that the mass-independent anomaly is carried by HO_2, though this is not a direct observation. It is still possible that the MIF observed in the present study comes from unexpected reactions not included in the present analysis. Thus, reaction 2 may be the source of the mass-independent isotopic anomaly. This possibility is reinforced by the water isotopic measurements. For the water samples produced in the high flow regime, when H_2O production exceeded H_2O_2 by a few orders of magnitude (i.e., no isotopic correction is needed), the isotopic ratios were directly observed. The results are plotted in Figure 7, along with the mass-dependent fractionation line and the mass-independent fractionation line obtained for H_2O_2. The water produced during these experiments is clearly mass independently fractionated, similar to H_2O_2. Since water is produced via OH radicals, which are produced from HO_2 (reactions 5a and 6−8), the same mass-independent anomaly is understandable if this anomaly is attributed to reaction 2.

The quantum dynamics of $H + O_2$ have been intensively studied [ref 52 and references therein] due to its importance in atmospheric and combustion chemistry. The reaction has two possible reactive channels (Figure 8). This spin-allowed reaction has no activation energy in the entrance channel. Studies show that the presence of even a small barrier in the incoming channel deteriorates agreement between calculated thermal rate constants and experiment.[53] Channel 1 is endothermic by 0.58 eV with respect to the asymptotic $H + O_2$ potential, making this reaction unimportant for our experiment (see kinetic chemistry section), while channel 2 is exothermic with a well depth minimum energy of −2.39 eV for HO_2. Two models of channel 2 have recently been reported, one using collisional recombination rate theory,[54] while the other utilizes the Chaperon mechanism for association rate constants.[55] Since both models assume conventional mass interaction (i.e., harmonic oscillator, collision rate) for the kinetic constant calculation, neither of them reproduces

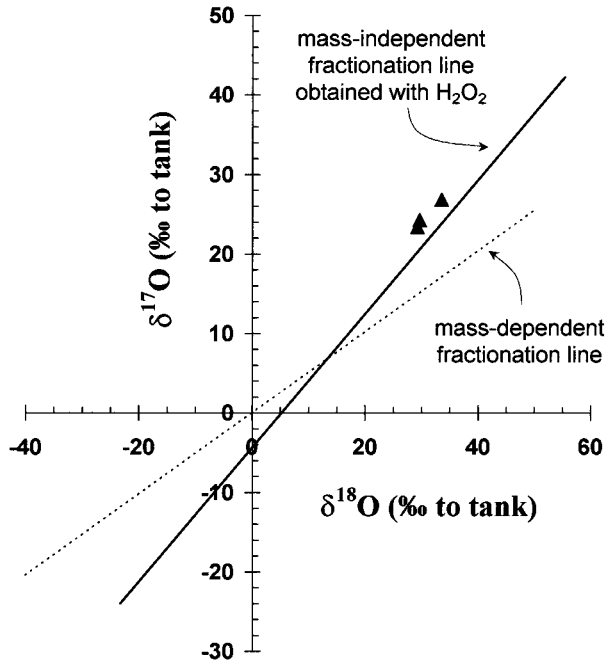

Figure 7. Water isotopic data in a three oxygen isotope plot along with the mass-dependent and mass-independent fractionation lines obtained from measurements displayed in Figure 4. The water data have been obtained at the high flow regime when $H_2O \gg H_2O_2$.

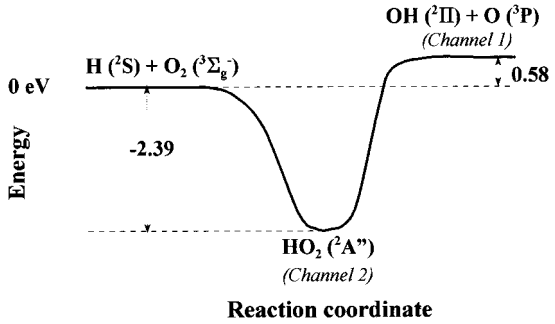

Figure 8. Schematic potential energy surface for $H + O_2$ (adapted from ref 52). Energies are in eV.

the present isotopic observations. Studies[56,57] have shown that the chain oxidation of organic compounds via repetitive sequence of two kinetic chain propagation reactions, $R + O_2 \rightarrow RO_2$ and $RO_2 + RO_2 \rightarrow 2RO + O_2$ produces mass independently fractionated oxygen. A nuclear spin (^{17}O) selectivity inducing molecular spin conversion of radical pairs was found to be the source of the mass-independent fractionation. However, in the present experiment, reaction 2 does not produce results predicted by this theory. Also, such reactions involve solution phase geminate recombination. Currently, no theory explains the mass-independent fractionation observed in a gas-phase chemical reaction. However, the similarity of isotopic behavior between HO_2 and ozone suggests a similar mechanistic origin. Recently, Mauersberger et al.[51] measured 15 of 18 possible reaction rates between O atoms and O_2 using the three stable oxygen isotopes. Their experiments question the role of molecular symmetry, though its involvement is not strictly ruled out. Collisions between light isotopes and heavy molecules can have rate coefficients as great as 50% above other combinations. Using the relative reaction rates, one can calculate a ratio of $k^{17}/k^{18} = 1.00$ for the isotopically most probable atmospheric reactions (i.e., only one heavy isotope involved in the reaction), in agreement with previous experiments at normal abundances.[2,5] This suggests that a similar isotope-dependent reaction rate

occurs in the $H + O_2$ reaction and, like ozone, the nature of the collision process in a third body reaction generates the mass-independent isotopic effect.

As observed by Bains-Sahota and Thiemens[43] for ozone formation in a flow system, a reverse isotopic effect at low flow is observed with $\delta^{17}O$ and $\delta^{18}O$ depleted in products. The best fit fractionation line does not pass through the initial isotopic composition for both studies. Bains-Sahota and Thiemens[43] suggested that diffusion, combined with heterogeneous wall reaction of O, should be a mass-dependent process and produce the observed shift of the data. This explanation is unlikely for the present work as all are performed in turbulent flow conditions, with both gases injected at high speed (105 m s^{-1} for H_2 and 0.7 m s^{-1} for O_2) and right angles. Since at low flow almost all injected O_2 is found in the products, it is possible that the water determines the isotopic composition of H_2O_2 and O_2*. This mass balance vanishes at high flow when the amount of O_2 is no longer the limiting reagent. Measurement of water samples produced from low flow condition experiments has confirmed this idea. Under these conditions water was enriched in ^{17}O when H_2O_2 and O_2* were depleted in ^{17}O.

Atmospheric Implications. HO_2 is part of the HO_x family, a dominant species in the chemistry of planetary atmospheres.[58] In the Earth's upper atmosphere (above 50 km), HO_x interacts strongly with the water cycle via photodissociation and interconversion. At these altitudes, reactions 5 and 8 are the main sinks of HO_2 and reaction 2, the source.[59,60] Therefore, the formation of HO_2 at these altitudes should produce a MIF component in the water vapor. In the troposphere, HO_2 is formed mainly by reaction 2 where the H atom derives from CO oxidation by OH. Hydroperoxide radicals ensure rapid conversion of NO to NO_2 in polluted areas, thus promoting ozone formation. In clean atmospheres, HO_2 reacts with O_3. The close connection between HO_2, O_3, and NO_2 and their ability to transfer an oxygen atom to other species should promote and propagate anomalous isotopic signatures in their byproducts, such as HNO_3. Disproportionation of HO_2 radicals in the atmosphere leads to the formation of hydrogen peroxide. Isotopic measurement of dissolved H_2O_2 in rainwater has already displayed a mass-independent character.[42] In light of the present experiments, the gas-phase production of H_2O_2 appears to be the source of MIF found in H_2O_2 dissolved in rainwater. A better understanding and characterization of this isotopic anomaly in the atmosphere, combined with the present observations will enhance understanding of oxygen chemistry in the atmosphere.

Summary and Conclusion

An oxygen isotopic study of H_x, O_x chemistry demonstrates a mass-independent isotopic fractionation. The main chemical behavior observed by Badin[41] and McKinley and Garvin[46] has been reproduced in the present study. It is observed that all of the products trapped at liquid nitrogen temperature are mass independently fractionated. Kinetic analysis of the reactions and variation of the reaction conditions lead to the suggestion that the source of the isotope effect is the $H + O_2 + M$ reaction, perhaps analogous to $O + O_2 + M$, however, no direct evidence of this suggestion is possible. The present results provide a new piece of the mass-independent fractionation puzzle. Since the discovery of this phenomenon in a chemical reaction in 1983, no consistent theory has emerged.

Acknowledgment. We thank the anonymous reviewers for their comments and J. Faquhar, S. K. Bhatacharya, and T. Jackson for helpful discussions during this work. This work was supported by the National Science Foundation.

References and Notes

(1) Venugopalan, M.; Jones, R. A. *Chemistry of dissociated water vapor and related systems*; Interscience Publishers: New York, 1968.
(2) Thiemens, M. H.; Heidenreich, J. E., III *Science* **1983**, *219*, 1073−1075.
(3) Mauersberger, K. *Geophys. Res. Lett.* **1987**, *14*, 80−83.
(4) Shueler, B.; Morton, J.; Mauersberger, K. *Geophys. Res. Lett.* **1990**, *17*, 1295−1298.
(5) Heidenreich, J. E., III; Thiemens, M. H. *J. Chem. Phys.* **1986**, *84*, 2129−2136.
(6) Thiemens, M. H.; Jackson, T. *Geophys. Res. Lett.* **1990**, *17*, 717−719.
(7) Bhattacharya, S. K.; H., T. M. *Z. Naturforcsh*. **1989**, *44A*, 435−444.
(8) Wen, J.; Thiemens, M. H. *J. Geophys. Res.* **1993**, *98*, 12,801−12,808.
(9) Gellene, G. I. *Science* **1996**, *274*, 1344.
(10) Yung, Y.; Lee, A. Y. T.; Irion, F. W.; DeMore, W. B.; J., W. *J. Geophys. Res.* **1997**, *102*, 10,857−10,866.
(11) Röckmann, T.; Brenninkmeijer, C. A. M.; Saueressig, G.; Bergamaschi, P.; Crowley, J. N.; Fisher, H.; Crutzen, P. J. *Science* **1998**, *281*, 544−546.
(12) Thiemens, M. H. *Science* **1999**, *283*, 341−345.
(13) Weston, R. E., Jr. *Chem. Rev.* **1999**, *99*, 2115−2136.
(14) Craig, H. *Geochim. Cosmochim. Acta* **1957**, *12*, 133−149.
(15) Matsuhisa, Y.; Goldsmith, J. R.; Clayton, R. N. *Geochim. Cosmochim. Acta* **1978**, *42*, 173−182.
(16) Cliff, S. S.; Thiemens, M. H. *Science* **1997**, *278*, 1774−1776.
(17) Thiemens, M. H.; Jackson, T.; Mauersberger, K.; Schueler, B.; Morton, J. *Geophys. Res. Lett.* **1991**, *18*, 669−672.
(18) Savarino, J.; Thiemens, M. H. "First measurement of both δ17O and δ18O oxygen isotopes in atmospheric hydrogem peroxide"; AGU Fall Meeting, 1997, San Francisco.
(19) Gunz, D. W.; R., H. M. *Atmos. Environ.* **1990**, *24A*.
(20) Sakuguwa, H.; Kaplan, I. R.; Tsai, W.; Cohen, Y. *Environ. Sci. Technol.* **1990**, *24*, 1452−1461.
(21) Hochanadel, C. J.; Sworski, T. J.; Ogren, P. J. *J. Phys. Chem.* **1980**, *84*, 3274−3277.
(22) Walch, S. P.; Duchovic, R. J. *J. Chem. Phys.* **1991**, *94*, 7068−7075.
(23) Kendrick, B.; Pack, R. T. *J. Chem. Phys.* **1995**, *102*, 1994−2012.
(24) Hsu, K. J.; Anderson, S. M.; Durant, J. L.; Kaufman, F. *J. Phys. Chem.* **1989**, *93*, 1018−1021.
(25) Hsu, K. J.; Durant, J. L.; Kaufman, F. *J. Phys. Chem.* **1987**, *91*, 1895−1899.
(26) Carleton, K. L.; Kessler, W. J.; Marinelli, W. J. *J. Phys. Chem.* **1993**, *97*, 6412−6417.
(27) Smith, H. A.; Kistiakowsky, G. B. *J. Am. Chem. Soc.* **1935**, *57*, 835−840.
(28) Smith, H. A.; Napravnik, A. *J. Am. Chem. Soc.* **1940**, *62*, 385−393.
(29) Atkinson, R.; Baulch, D. L.; Cox, R. A.; Hampson, R. F., Jr.; Kerr, J. A.; Rossi, M. J.; Troe, J. *J. Phys. Chem. Ref. Dat.* **1997**, *26*, 1329−1499.
(30) Hanning-Lee, M. A.; Pilling, M. J.; Warr, J. F. *J. Chem. Soc., Faraday Trans.* **1991**, *87*, 2907−2912.
(31) Baulch, D. L.; Cobos, C. J.; Cox, R. A.; Frank, P.; Hayman, G.; Just, T.; Kerr, J. A.; Murrels, T.; Pilling, M. J.; Troe, J.; Walker, R. W.; Warnatz, J. *J. Phys. Chem. Ref. Dat.* **1994**, *23*, 847−1033.
(32) Arnau, J. L.; Giguère, P. A. *Can. J. Chem.* **1972**, *51*, 1525−1529.
(33) Deglise, X.; Giguère, P. A. *Can. J. Chem.* **1971**, *49*, 2242−2247.
(34) Giguère, P. A.; Herman, K. *Can. J. Chem.* **1970**, *48*, 3473−3482.
(35) Giguère, P. A. *J. Phys. Chem.* **1981**, *85*, 3733−3734.
(36) Ardon, M. *Oxygen*; Benjamin, W. A. Inc.: New York, 1965.
(37) Cahill, A. E.; Taube, H. *J. Am. Chem. Soc.* **1952**, *74*, 2312−2318.
(38) Anbar, M.; Guttman, S. *J. Am. Chem. Soc.* **1961**, *83*, 2035−2037.
(39) Schumb, W. C.; Satterfield, C. N.; Wentorth, R. L. *Hydrogen Peroxide*; Reinhold: New York, 1955.
(40) Holt, B. D.; Kumar, R. *Anal. Chem.* **1987**, *59*, 995−999.
(41) Badin, E. J. *J. Am. Chem. Soc.* **1948**, *70*, 3651−3655.
(42) Savarino, J.; Thiemens, M. H. *Atmos. Environ.* **1999**, *33*, 3683−3690.
(43) Bains-Sahota, S. K.; Thiemens, M. H. *J. Phys. Chem.* **1987**, *91*, 4370−4374.
(44) Bhattacharya, S. K.; Savarino, J.; Thiemens, M. H. *Science* **1999**, submitted for publication.
(45) Geib, K. H.; Harteck, P. *Z. Physik. Chem.* **1934**, *170*, 1.
(46) McKinley, J. D.; Garvin, D. *J. Am. Chem. Soc.* **1955**, *77*, 5802−5805.

(47) Avramenko, L. I.; Kolesnikova, R. V. *Russ. J. Phys. Chem.* **1959**, *33*, 515−518.
(48) Du, H.; Hessler, J. P. *J. Chem. Phys.* **1992**, *96*, 1077.
(49) Niki, P. D.; Savage, C. M.; Breitenbach, L. P. *Chem. Phys. Lett.* **1980**, *73*, 43−46.
(50) Mozurkewich, M.; Benson, S. W. *Int. J. Chem. Kinet.* **1985**, *17*, 787−807.
(51) Mauersberger, K.; Erbacher, B.; Krankowsky, D.; Günther, J.; Nickel, R. *Science* **1999**, *283*, 370−372.
(52) Meijer, A. J. H. M.; Goldfield, E. M. *J. Chem. Phys.* **1999**, *110*, 870−880.
(53) Barone, V. *J. Chem. Phys.* **1994**, *101*, 10666−10675.
(54) Mandelshtam, V. A.; Taylor, H. S.; Miller, W. H. *J. Chem. Phys.* **1996**, *105*, 496−503.
(55) Varandas, A. J. C.; Pais, A. A. C. C.; Marques, J. M. C.; Wang, W. *Chem. Phys. Lett.* **1996**, *249*, 264−271.
(56) Buchachenko, A. L. *Chem. Rev.* **1995**, *95*, 2507−2528.
(57) Buchachenko, A. L.; Yasina, L. L.; Belyakov, V. A. *J. Phys. Chem.* **1995**, *99*, 4964−4969.
(58) Yung, Y. L.; DeMore, W. B. *Photochemistry of planetary atmosphere*; Oxford University Press: New York, 1999.
(59) Torr, D. G. The photochemistry of the upper atmosphere. In *The photochemistry of atmosphere*; Levine, J. S., Ed.; Academic Press Inc.: New York, 1985; pp 165−276.
(60) Brasseur, G.; Solomon, S. *Aeronomy of the middle atmosphere*, 2nd ed.; Reidel: Norwell, MA, 1986.